Journal of Medicinal Chemistry

Article

pubs.acs.org/jmc

Identification of a Novel Family of BRAF^{V600E} Inhibitors

Jie Qin,[†] Peng Xie,[†,‡] Christian Ventocilla,[‡] Guoqiang Zhou,[‡] Adina Vultur,[†] Quan Chen,[†] Qin Liu,[†] Meenhard Herlyn,[†] Jeffrey Winkler,*[,‡] and Ronen Marmorstein*[,†,‡]

[†]The Wistar Institute and [‡]Department of Chemistry, University of Pennsylvania, Philadelphia, Pennsylvania 19104, United States

Supporting Information

ABSTRACT: The BRAF oncoprotein is mutated in about half of malignant melanomas and other cancers, and a kinase activating single valine to glutamate substitution at residue 600 (BRAF^{V600E}) accounts for over 90% of BRAF-mediated cancers. Several BRAF^{V600E} inhibitors have been developed, although they harbor some liabilities, thus motivating the development of other BRAF^{V600E} inhibitor options. We report here the use of an ELISA based high-throughput screen to identify a family of related quinolol/naphthol compounds that preferentially inhibit BRAF^{V600E} over BRAF^{WT} and other kinases. We also report the X-ray crystal structure of a BRAF/quinolol complex revealing the mode of inhibition, employ structure-based medicinal chemistry efforts to prepare naphthol analogues that inhibit BRAF^{V600E} in vitro with IC_{50} values in the 80−200 nM range under saturating ATP concentrations, and demonstrate that these compounds inhibit MAPK signaling in melanoma cells. Prospects for improving the potency and selectivity of these inhibitors are discussed.

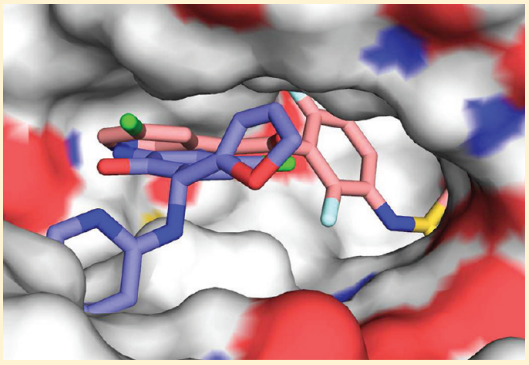

INTRODUCTION

RAF family kinases are central players in the highly conserved MAPK signaling pathway (RAS-RAF-MEK-ERK), which relay signals from the extracellular space through receptor tyrosine kinases (RTKs) to the nucleus to promote the expression of genes involved in cell proliferation and survival. RAF kinases function by specifically phosphorylating MEK1/2 on the kinase activation loop, leading to the subsequent activation of ERK1/2.[1] The three isoforms of the RAF kinases, ARAF, BRAF, and CRAF, share a common three-domain structure containing the conserved regions CR1, CR2, and CR3. The regulation of RAF kinase activity is complex and involves a variety of different kinases and scaffolding proteins.[1] However, compared to ARAF and CRAF, BRAF requires fewer regulation events for its activation. Due to this property, BRAF has significantly higher basal activity than the other RAF family isoforms and has also been found to be a major activator of MEK1/2.[2,3]

BRAF is an important oncogene that is mutated in about a half of malignant melanomas and at a lower frequency in a wide range of other human cancers, such as thyroid, colon, ovarian, lung, and breast cancers.[4,5] Oncogenic mutations occur within the kinase domain, with a single valine to glutamate substitution at residues 600 (BRAF^{V600E}) accounting for over 90% of these mutations.[1,4,6,7] Because of these findings, BRAF, and BRAF^{V600E} in particular, has emerged as an attractive anticancer drug target. A number of inhibitors against BRAF have been developed so far and more are at various stages of preclinical and clinical development.[8−11] For example, vemurafenib (PLX4032), an azaindole compound and orally available ATP competitive BRAF inhibitor that shows selectivity for BRAF^{V600E}, has received FDA approval for the treatment of late stage metastatic melanoma.[12] Encouragingly, in phase III clinical trials, PLX4032 produced 2 complete responses and 24 partial responses out of 32 patients, extending life in many cases by more than 6 months, prior to the eventual development of drug resistance through reactivation of the MAPK pathway or through the activation of alternative compensatory pathways, involving receptor tyrosine kinases (RTKs), PI3K-AKT, and other pathways.[13,14] However, about half of the patients had the drug dose reduced, and nearly two-thirds had to have their treatments temporarily stopped because of side effects.[9,10] In addition, approximately one-quarter of patients developed cancerous or precancerous nonmelanoma skin lesions.[9,10] Given these limitations of vemurafenib, and some other drugs that are being evaluated to treat metastatic melanoma, it would be useful to have additional BRAF^{V600E} inhibitor drug options for some patients.

Here, we report the development of an ELISA-based high-throughput assay to screen a combined diverse library of over 30,000 organic compounds for BRAF^{V600E} inhibition. This screen, the structure determination of BRAF bound to one of the identified inhibitors, and the follow-up structure-based medicinal chemistry efforts resulted in the identification of a family of related compounds containing a quinolol or naphthol backbone that selectively inhibit BRAF^{V600E} over BRAF^{WT} in vitro, display IC_{50} values in the 80−200 nM range under saturation ATP concentrations, and inhibit MAPK signaling in melanoma cells.

RESULTS

Identification of a Novel Family of BRAF^{V600E} Inhibitors. In order to screen for BRAF inhibitors in a high-throughput

Received: February 11, 2012
Published: April 26, 2012

   dx.doi.org/10.1021/jm3004416 | J. Med. Chem. 2012, 55, 5220−5230

format, we employed an Enzyme-Linked Immunosorbent Assay (ELISA)-based system that was previously used by others[15] and us.[16] The details of the assay were essentially as described previously.[16] Briefly, we carried out the screen in a 96-well microtiter plate containing covalently immobilized glutathione to enable the capture of glutathione-*S*-transferase (GST) fusion protein (Pierce Biotechnology) linked to the full-length MEK protein. A mouse monoclonal antibody recognizing BRAF-phosphorylated residues on MEK is then added to the microtiter plate to bind the immobilized and phosphorylated GST-MEK. Antibody molecules that are nonspecifically bound are then washed away, and horseradish peroxidase (HRP) linked IgG is added to bind to the primary antibody. The amount of HRP IgG binding is then quantified by measuring the chemiluminescence generated by the mixing of the HRP substrate with specifically bound HRP IgG. As shown in Figure 1A, a Z′ factor

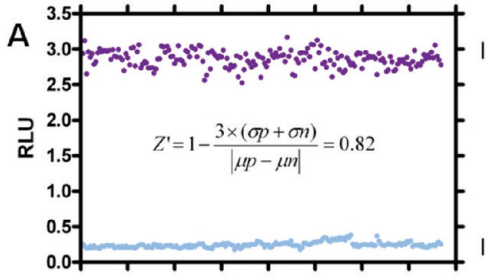

B

Libraries	Compounds
DOS Library	6,081
Commercial	9,006
Bioactive	1,496
Natural Products	2,015
Academic	761
Kinase set	12,617
Total	**31,976**

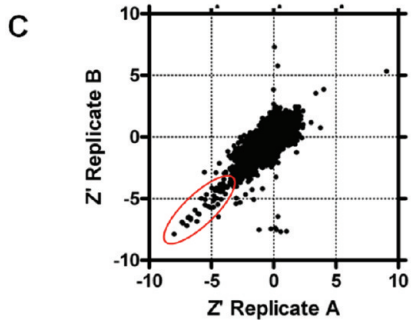

Figure 1. Screen for small molecule $BRAF^{V600E}$ inhibitors. (A) Z′ factor test for the BRAF ELISA-based enzymatic assay system. (B) Summary of small molecule libraries that were screened. (C) Scatter plot of the HTS in replicates against a combined library of 31,976 small molecule compounds. Inhibitors that were analyzed further are circled.

of 0.82 was obtained indicating that this BRAF ELISA-based assay was effective for high throughput screening.

We used the ELISA-based HTS system to screen a combined library of 31,976 diverse compounds (at a compound concentration of 5 μM, a $BRAF^{V600E}$ concentration of 140 nM, and a saturating ATP concentration of 100 μM) (Figure 1B and C). From this library, the 23 top scoring compounds deemed to have drug-like properties were purchased directly from their corresponding vendors and were confirmed in a repeat assay to inhibit $BRAF^{V600E}$ activity to more than 90% at an inhibitor concentration of 5 μM (Figure S1A, Supporting Information and compounds **1**−**23** in Figure S1B, Supporting Information). Encouragingly, a known CRAF inhibitor was identified in three independent libraries (**15** in Figure S1B, Supporting Information) and scored among the top 30 inhibitor hits from this experiment, confirming the efficacy of this assay system.

Upon close examination of the representative scaffolds with a rough filtration according to Lipinski's rule of five,[17] 23 compounds were determined to display drug-like structures (compounds **1**−**23** in Figure S1B, Supporting Information). Notably, seven of the compounds contained a quinolol, naphthol, or related substructure (compounds **1**, **2**, **3**, **6**, **7**, **16**, and **17** in Figure S1B, Supporting Information). Given that this was the largest set of related compounds that we identified in our screen and that these compounds were not previously identified as kinase inhibitors, we focused on their further analysis.

Five of these quinolol/naphthol analogues, in addition to two other closely related compounds (compounds **4** and **5**) (Figure 2A), were further characterized by measuring dose−response curves for their inhibition against both $BRAF^{WT}$ and $BRAF^{V600E}$ at a protein concentration of 30 nM and inhibitor concentrations ranging from 10 μM to 5 nM to approximate their IC_{50} values (Figure 2A). This analysis revealed that the most potent inhibitor from these series, **2**, inhibited $BRAF^{V600E}$ with an IC_{50} value of about 100 nM and with about a 3-fold selectivity for $BRAF^{V600E}$ over $BRAF^{WT}$. Each of the other related inhibitors also displayed strong inhibition toward $BRAF^{V600E}$ with IC_{50} values within the submicromolar range. All but **5** showed a 2−5-fold selectivity for $BRAF^{V600E}$ over $BRAF^{WT}$.

Crystal Structure of a Quinolol Analogue in Complex with the BRAF Kinase Domain. In order to understand the mode of action of this family of BRAF inhibitors, cocrystallization of the BRAF kinase domain (BRAF-KD, residues 433−726) with several of the inhibitors was attempted. Since the MALDI-TOF mass spectrum data of BRAF-KD expressed and purified from Sf9 insect cells indicated that the protein is extensively phosphorylated, lambda protein phosphatase (λPP) treatment was used to generate homogeneous hypophosphorylated protein samples for cocrystallization. Extensive cocrystallization efforts using the microbatch method produced cocrystals with only **1** with the wild-type BRAF kinase domain. Crystals of the complex were small (300 μm × 30 μm × 30 μm) producing only low resolution data using a home X-ray source, but data to about 2.5 Å resolution could be obtained using a 10 μm mini-beam at the Advanced Photon Synchrotron source. The BRAF-KD/**1** structure was determined by molecular replacement using the unliganded BRAF-KD/sorafenib crystal structure (PDB accession code: 1UWH) as a search model. The BRAF-KD/**1** crystals contained two copies of the BRAF-KD/**1** complex in one asymmetric unit cell. Electron density corresponding to inhibitor **1** was visible in the ATP binding pockets of both molecules in the asymmetric unit cell. The structure was refined with strict NCS symmetry imposed with the inhibitor modeled only at the later stages of refinement. The final structure was determined to 2.55 Å resolution to an R_{work}/R_{free} of 0.2203/0.2659 with good geometry (Table 1).

The BRAF-KD/**1** structure revealed that the inhibitor binds within the ATP binding cleft between the N-lobe and C-lobe of the kinase domain, and an overlay with the structure of PKA in complex with ATP revealed significant overlap of **1** with both

dx.doi.org/10.1021/jm3004416 | *J. Med. Chem.* 2012, 55, 5220−5230

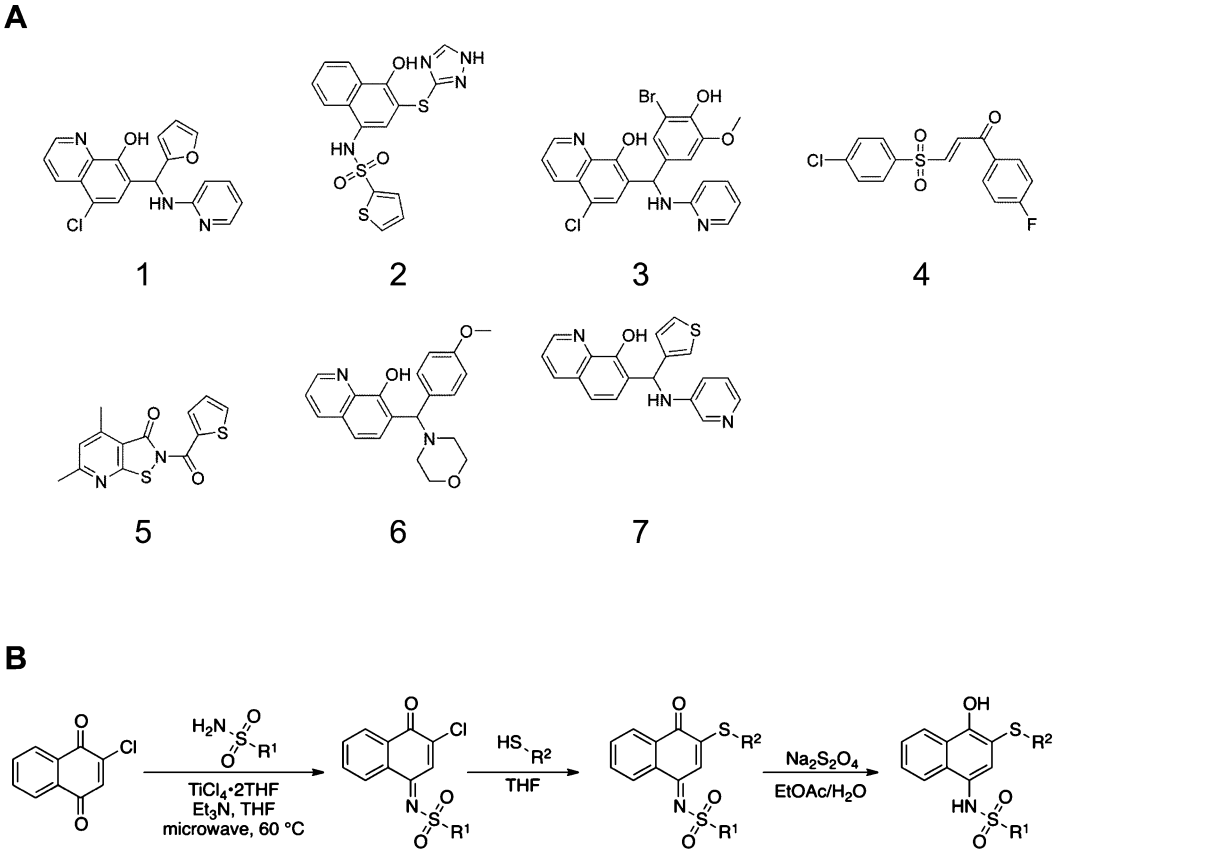

Figure 2. Family of quinolol and naphthol BRAF^{V600E} inhibitors. (A) Structures of selected HTS inhibitors that share a common scaffold. Single measurment dose−response inhibition curves were carried out for each of the cherry-picked compounds to approximate their IC_{50} values (μM) as follows: **1** (BRAF^{WT}= 0.8, BRAF^{V600E} = 0.4), **2** (BRAF^{WT} = 0.3, BRAF^{V600E} = 0.1), **3** (BRAF^{WT} = 3.0, BRAF^{V600E} = 0.7), **4** (BRAF^{WT} = 0.9, BRAF^{V600E} = 0.3), **5** (BRAF^{WT} = 0.4, BRAF^{V600E} = 0.6), **6** (BRAF^{WT} = 4.0, BRAF^{V600E} = 0.9), and **7** (BRAF^{WT} = 2.0, BRAF^{V600E} = 0.8). (B) General scheme for the synthesis of analogues of **2**.

Table 1. Crystallographic Data Collection and Refinement Statistics for the BRAF/1 Complex

Data Collection	
complex	BRAF−1
space group	$P4_12_12$
cell dimensions	
a, *c* (Å)	94.3, 163.5
resolution (Å)	50−2.55
R_{merge} [a]	0.155 (0.660)
$I/\sigma(I)$	19.6 (2.3)
completeness (%)	99.8% (97.8%)
multiplicity	13.0 (5.1)
Refinement	
R_{work} [b]/R_{free} [c]	0.2203/0.2659
rmsd	
bond lengths (Å)	0.0073
bond angles (deg)	1.36

[a]Highest resolution shell is shown in parentheses. $R_{merge} = \Sigma_{hkl}\ |I(hkl) - \langle I(hkl)\rangle|/\Sigma_{hkl}(hkl)$, where $\langle I(hkl)\rangle$ is the mean of the symmetry-equivalent reflections of I(hkl). [b]$R_{work} = \Sigma||F_o| - |F_c||/|F_o|$. [c]$R_{free} = \Sigma_T||F_o| - |F_c||/\Sigma_T|F_o|$ (where T is a test data set of 9.3% of the total reflections randomly chosen and set aside before refinement).

the adenine and the ribose moieties of the ATP molecule (Figure 3A). The activation loop of BRAF bound to **1** takes on the active conformation that is observed with BRAF in complex with the PLX4720 (Figure 3B)[18] and CS292[19] inhibitors as opposed to the inactive conformation that is observed with BRAF bound to sorafenib (Figure 3C).

The R-stereoisomer of **1** appears to be bound to the BRAF ATP binding pocket. The quinoline ring is stacked between the N- and C-lobes and against the kinase hinge region with the chloride atom pointing toward the DFG loop with the furan pointing toward the P-loop and the pyridine pointing in the opposite direction toward the D helix (Figure 4A). Specifically, the quinolinol moiety of **1** is intercalated into the space between residues Trp531 and Phe583 forming $\pi-\pi$ stacking interactions (Figure 4B). In addition, the nitrogen atom of the quinoline ring of **1** forms hydrogen-bonding interactions with the hinge region of the N- and C-lobes, potentially through the bridging of a water molecule to the main chain carbonyl of residue Cys532. There are also extensive van der Waals contacts between **1** and other residues in the protein pocket such as residues Ile463, Val471, Ala481, Gly464, Thr529, Gln530, Ser535, Ser536, His539, Asn580, Asn581, and Gly593. The furan group is pointing to the extension of the P-loop, and the pyridine group is in proximity to His539 of the αD helix. Similar to other BRAF/inhibitor structures with the protein in the active conformation, an 11 Å long "Raf specificity pocket" that is defined by the DFG motif sequence and the αC helix is lined by residues Thr529 (the gatekeeper residue), Leu505, Leu514, Gly593, Asp594, and Phe595[18] (Figure 4C). Taken together, structural evidence reveals extensive and specific interactions between **1** and the ATP binding pocket of the BRAF kinase domain, establishing **1** as a Type I inhibitor,

dx.doi.org/10.1021/jm3004416 | J. Med. Chem. 2012, 55, 5220−5230

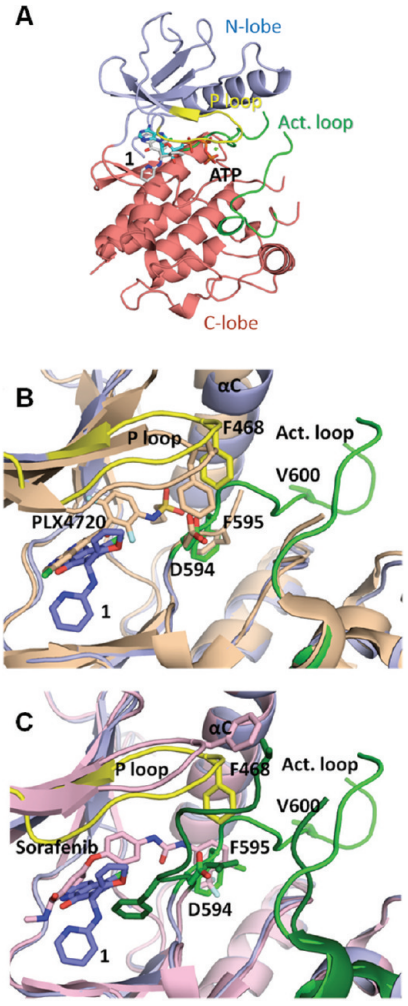

Figure 3. Crystal structure of BRAF in complex with compound **1**. (A) Overall structure of the BRAF kinase domain in complex with **1**. The N-lobe, C-lobe, P-loop, and activation loop (Act. loop) of the kinase domain are color coded blue, red, yellow, and green, respectively. Compound **1** is shown in a white stick and ball model. The ATP molecule from the PKA/ATP complex structure is overlaid with BRAF/**1** to show the binding of ATP in the BRAF kinase active site. The ATP model is shown in yellow for the adenine and ribose fragments and in orange for the phosphates. The same color coding scheme is preserved in all panels of this figure. (B) Overlay of active sites of BRAF in complex with **1** (blue) and PLX4720 (orange) (PDB ID: 3C4C) revealing conserved "active" kinase conformations. Key residues of the active site for transition into the active conformation (F468, D594, F595, and V600 are highlighted). (C) Overlay of active sites of BRAF in complex with **1** (blue) and sorafenib (pink) in the inactive conformation (PDB ID: 1UWH). The conformation of the activation loop of the active BRAF and inactive sorafenib complexes are shown in light and dark green, respectively. All structural superpositions were generated by overlaying the Cα positions of various kinase structures using secondary structure matching (SSM) in Coot.[33]

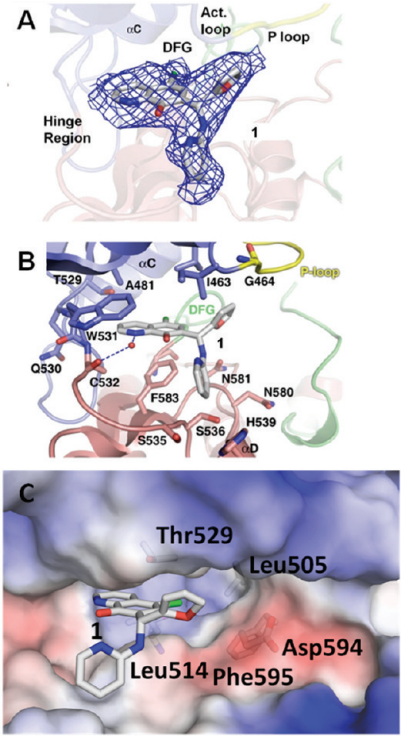

Figure 4. Details of the BRAF-1 interface. (A) Electron density generated from a simulated annealing $F_o - F_c$ map in which the inhibitor was omitted from the refinement is shown contoured at 4σ. Key active site regions of the kinase are also highlighted. (B) Interactions between **1** and BRAF active site residues. Hydrogen bonding interactions are represented by blue dashed lines, and residues that mediate van der Waals interactions with inhibitor are also highighted. (C) Electrostatic potential surface of the BRAF/**1** complex structure highlighting the inhibitor as a stick figure.

binding to the ATP pocket in the active conformation, confirming its inhibition properties against both $BRAF^{WT}$ and $BRAF^{V600E}$.

Preparation and Characterization of a Focused BRAF Inhibitor Library. Of the family of quinolol/naphthol BRAF inhibitors that were identified in the screen, we carried out a structure–activity relationship (SAR) around **2** (Figure 2A) because it was the most potent $BRAF^{V600E}$ inhibitor identified in our screen, and it appeared to be most tractable for medicinal chemistry efforts. On the basis of the BRAF-KD/**1** structure and the similarity between inhibitors **1** and **2** (Figure 2A), we hypothesized that the naphthol heterocycle of **2** would occupy the same space as the quinolol of **1** with the thiotriazole and the thienylsulfonamide of **2** occupying the positions of the furan/aminopyridine and chloride groups of **1**, respectively. On the basis of this hypothesis, we resynthesized **2** and prepared a total of 38 compounds, varying the nature of both the nitrogen-containing heterocycle corresponding to the thiotriazole ring and the sulfonamide substitution in **2**. The general scheme for the synthesis of these compounds is shown in Figure 2B. We then screened each of these analogues against $BRAF^{V600E}$ and $BRAF^{WT}$ (at protein and ATP concentrations of 28 nM and 100 μM, respectively) using a dose–response curve to calculate IC_{50} values.

As can be seen in Figure 5 and Table 2, resynthesized **2** shows IC_{50} values for $BRAF^{V600E}$ and $BRAF^{WT}$ of 0.17 μM and 0.26 μM, respectively, close to the values of 0.11 μM and 0.32 μM obtained for the screen compound. To further confirm our modeling of **2** into the ATP binding site of $BRAF^{WT}$ based on the $BRAF^{WT}$/**1** structure, we prepared the oxidized form of **2** (compound **24**). On the basis of this modeling, we hypothesized that the OH group of the naphthol points into solvent, so the inhibitor potency would therefore be insensitive to its oxidation state. Our data showed that **2** and **24** show comparable potencies for $BRAF^{WT}$ and $BRAF^{V600E}$ (Table 2). This is consistent with our hypothesis. Nonetheless, it is

dx.doi.org/10.1021/jm3004416 | J. Med. Chem. 2012, 55, 5220–5230

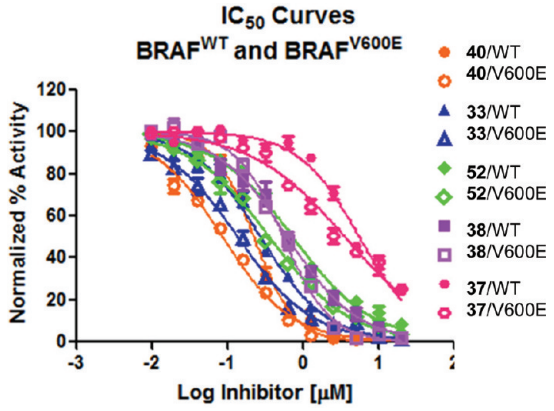

Figure 5. IC_{50} curves for compound **2** analogues against $BRAF^{WT}$ and $BRAF^{V600E}$. Dose–response inhibition curves of selected compounds are shown and plotted as normalized percent activity.

possible that the assay conditions may regenerate the oxidized form, therefore leaving open the possibility that $BRAF^{WT}$/$BRAF^{V600E}$ actually binds to the oxidized form of the naphthol analogues prepared in this study.

A SAR of the other naphthol analogues of **2** reveals that, as expected, other substitutions on the naphthol ring system have significant effects on inhibitor potency for $BRAF^{V600E}$ (Table 2 and Table S1, Supporting Information). Specifically, replacement of the thiotriazole present in **2** with a hydrogen atom reduced potency by more than 30-fold (compare **2** with **25**), whereas replacement of the thiotriazole with a halogen only reduced binding by about 3-fold (compare **2** with **26** and **27**). In contrast, several different heterocycles at this position can be accommodated (**28**–**31**), while another compound is more poorly accommodated (**32**). The structure of the BRAFWT/**1** complex suggests that the thiotriazole of modeled **2** would be pointing out toward the solvent of the enzyme where the protein substrate would bind suggesting that these substitutions may have differential effects on substrate binding. Substitution of the sulfonamide that presumably occupies the RAF-specific pocket also has significant effects on inhibitor potency. Specifically, sulfonamides that contain a functionalized aryl group (for example, **33**, **34**, **40**, and **41**) are significantly more potent than sulfonamides containing long aliphatic groups (for example, **35** and **36**). In addition, highly substituted aryls in the sulfonamide moiety significantly decrease inhibitor potency by 3- to 20-fold (for example, **37**–**39**). We hypothesize that the highly substituted aryls or long aliphatic groups are too bulky or long, respectively, to be accommodated by the $BRAF^{WT}$/$BRAF^{V600E}$ specificity pocket. The most potent $BRAF^{V600E}$ inhibitors identified were **28** (IC_{50} = 0.12 μM), **44** (IC_{50} = 0.14 μM), and **40** (IC_{50} = 0.08 μM) (Figure 5 and Table 2). Each of these inhibitors exhibited about a 2-fold selectivity for $BRAF^{V600E}$ over $BRAF^{WT}$.

Table 2. Structures and IC_{50} Values of Naphthol Inhibitor Analogues against $BRAF^{WT}$ and $BRAF^{V600E}$[a]

Compound	R¹	R²	IC_{50} (95% confidence interval)[b] $BRAF^{WT}$ (uM)	IC_{50} (95% confidence interval)[b] $BRAF^{V600E}$ (uM)
2			0.26 (0.24 to 0.28)	0.17 (0.14 to 0.19)
24	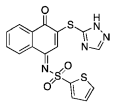		0.23 (0.21 to 0.25)	0.19 (0.17 to 0.21)
25		H	9.0 (8.2 to 10)	6.1 (5.0 to 7.3)
26		Cl	0.45 (0.39 to 0.51)	0.38 (0.33 to 0.44)
27		Br	0.34 (0.30 to 0.39)	0.32 (0.27 to 0.39)
28			0.17 (0.16 to 0.19)	0.12 (0.11 to 0.14)
29			0.35 (0.30 to 0.40)	0.19 (0.16 to 0.24)
30			0.32 (0.30 to 0.33)	0.25 (0.20 to 0.30)
31			0.57 (0.48 to 0.66)	0.28 (0.24 to 0.33)
32			1.47 (1.27 to 1.72)	0.72 (0.57 to 0.91)
33			0.27 (0.25 to 0.30)	0.14 (0.12 to 0.15)

Compound	R¹	R²	IC_{50} (95% confidence interval)[a] $BRAF^{WT}$ (uM)	IC_{50} (95% confidence interval)[a] $BRAF^{V600E}$ (uM)
34			0.19 (0.15 to 0.24)	0.21 (0.18 to 0.24)
35			2.1 (1.7 to 2.6)	1.6 (1.4 to 1.7)
36			1.66 (1.56 to 1.77)	0.72 (0.60 to 0.86)
37	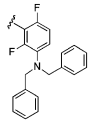		5.8 (4.9 to 6.8)	3.6 (2.8 to 4.6)
38			0.59 (0.51to 0.68)	0.52 (0.46 to 0.58)
39			0.68 (0.61 to 0.77)	0.67 (0.55 to 0.80)
40			0.22 (0.20 to 0.25)	0.08 (0.07 to 0.09)
41			0.40 (0.29 to 0.52)	0.15 (0.12 to 0.19)

[a]Compounds **3**–**23** are listed in Figure S1B (Supporting Information) and compounds **42**–**61** are listed in Table S1 (Supporting Information). [b]The 95% confidence interval of IC_{50} was calculated as the antilog of the upper and lower limits of the 95% confidence interval of Log IC_{50}.

dx.doi.org/10.1021/jm3004416 | J. Med. Chem. 2012, 55, 5220–5230

Characterization of BRAF Inhibitor 40 in Vitro and in Melanoma Cells. In order to survey the selectivity of the most potent $BRAF^{V600E}$ inhibitor, **40**, we profiled the compound against 7 other randomly chosen kinases representing each of the 6 major groups of serine−threonine kinases; PAK1 (STE group), PIM1 (CAMK group), GSK3 (CMGC group), p70S6K (AGC group), PI3Kα and PI3Kγ (CK1 group), and the BRAF related CRAF kinase (TKL group), at an inhibitor concentration of 1 μM. This analysis revealed that **40** showed significant selectivity for $BRAF^{V600E}$ and $BRAF^{WT}$ over the other kinases (Figure 6A). While $BRAF^{V600E}$ and $BRAF^{WT}$ both showed less than 10% remaining activity, CRAF showed about 60% remaining activity, while the other kinases showed 75% or greater remaining activity. Taken together, these data demonstrates that **40** has significant selectivity for $BRAF^{V600E}$ and $BRAF^{WT}$ over representative kinases from the other major groups of serine−threonine kinases.

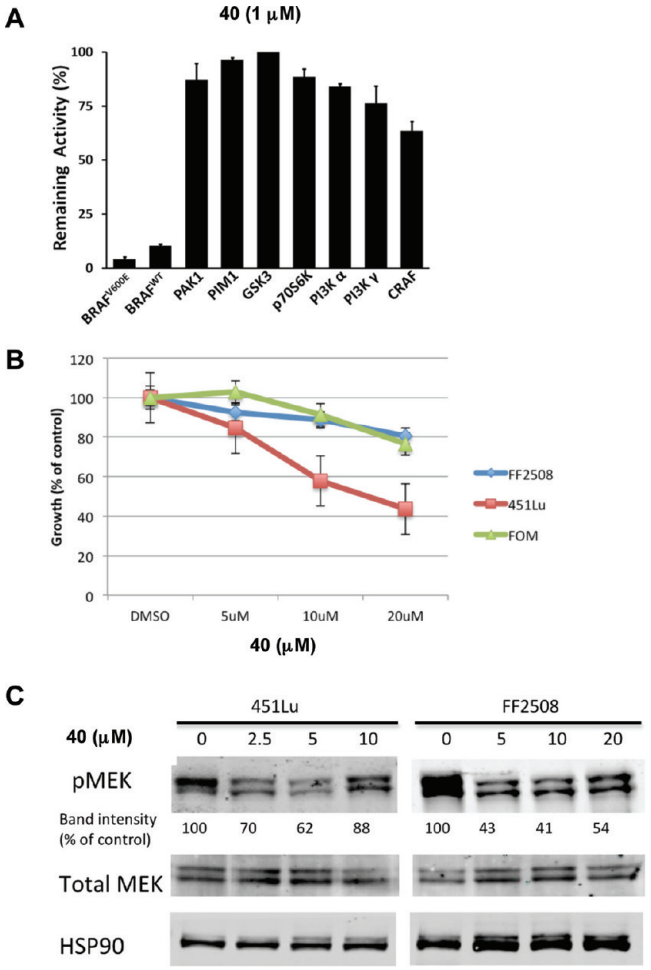

Figure 6. In vitro kinase selectivity and melanoma cell response to compound **40**. (A) Activity of **40** against 7 other randomly chosen kinases (indicated) at an inhibitor concentration of 1 μM. Data is shown as the mean ± SEM (n = 3). (B) Dose−response growth inhibition curves of human melanocytes (FOM), fibroblasts (FF2508), and a melanoma cell line (451Lu) in the presence of increasing doses of **40**. Data are shown as the mean ± SD (n = 4) and are representative of three independent experiments. (C) 451Lu melanoma cells were treated with increasing concentrations of **40**. Cell lysates were analyzed by immunoblotting with the indicated antibodies.

We further investigated the effects of **40** in the context of human-derived skin and melanoma cells. A proliferation assay indicated that a mutant BRAF melanoma cell line (451Lu, harboring a $BRAF^{V600E}$ mutation) is more sensitive to the compound than its normal melanocyte and fibroblast counterparts (Figure 6B). Western blot analyses further indicated that MAPK pathway activity is decreased, as evidenced by reduced phospho-MEK levels in the presence of the inhibitor, compared to the vehicle control treated cells (Figure 6C).

■ DISCUSSION AND CONCLUSIONS

In this study, we report on developing an ELISA based high-throughput assay that is suitable for screening a large library of small molecule compounds for inhibition of BRAF kinase activity. We employed this assay to screen a combined diverse library of over 30,000 organic compounds for $BRAF^{V600E}$ inhibition. Of the inhibitors that were identified, we further pursued a family of related quinolol and naphthol compounds that appeared to represent a novel family of $BRAF^{V600E}$ inhibitors. We then determined the X-ray crystal structure of one of these inhibitors bound to the BRAF kinase domain revealing that the compounds bind in the ATP binding cleft of the kinase in its active conformation. This structure was used as a scaffold to initiate a medicinal chemistry campaign that resulted in the preparation of a family of naphthol compounds that selectively inhibit $BRAF^{V600E}$ over $BRAF^{WT}$ in vitro with IC_{50} values in the 80−200 nM range in the presence of saturating levels of ATP. We also demonstrated that one of these compounds, **40**, has significant selectivity for $BRAF^{V600E}$ and $BRAF^{WT}$ over other kinases and inhibits MAPK signaling in melanoma cells.

The medicinal chemistry campaign revealed that substitutions on the naphthol ring system had significant effects on inhibitor potency for $BRAF^{V600E}$. Most significantly, substitutions in the naphthol ring system corresponding to the thienylsulfonamide present in **2** (the most potent compound obtained from the primary screen) had the most dramatic effects on inhibitor potency (Table 2 and Table S1, Supporting Information). Modeling of **2** onto the X-ray structure of the BRAF-KD/**1** complex (where the thienylsulfonamide of **2** overlays with the chloride group of **1**) suggests that this sensitive position of the inhibitor points into a pocket that is unique to BRAF kinase (Figure 4C). Indeed, the superposition of the BRAF complexes with **1** and PLX4720 confirms this, as it reveals that the chloride group of **1** points toward the sulfonamide group of PLX4720 that sits in the BRAF specificity pocket (Figure 7). In light of this, it is not a surprise that different sulfonamides at this position on the backbone of **2** have dramatic effects on inhibitor potency, with sulfonamides that contain a functionalized aryl group yielding more potent inhibitors than sulfonamides containing long aliphatic groups. Clearly, the preparation of other sulfonamide analogues of **2** might yield more potent inhibitors, and hybrid molecules containing the **2** backbone with the sulfonamide derivative of PLX4720 could provide particularly potent and selective $BRAF^{V600E}$ inhibitors.

Initial in vitro and cell-based assays indicate that our current approach yielded a BRAF/$BRAF^{V600E}$ selective inhibitor (**40**) that reduces melanoma cell proliferation preferentially over primary fibroblasts and melanocytes. However, the downstream effector of BRAF (MEK) appears to be inhibited regardless of the cells' transformation or BRAF status. It is therefore possible that these inhibitors might be hitting other pathways in cells that are important for melanoma cell proliferation, and broader kinase profiling and cell based studies would have to be carried

dx.doi.org/10.1021/jm3004416 | J. Med. Chem. 2012, 55, 5220−5230

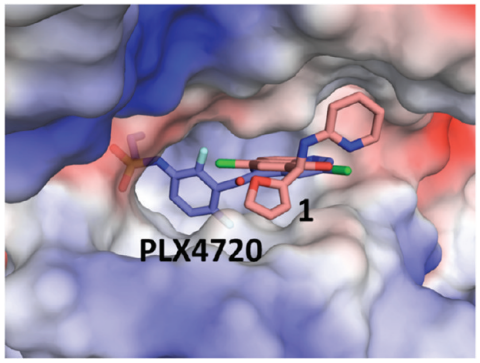

Figure 7. Superposition of compound **1** and PLX4720 bound to BRAF. The inhibitors are shown as stick figures with the protein shown as an electrostatic surface highlighting the RAF specificity pocket that is accessible off the chlorine atom of **1**.

out to address this possibility. In addition, our cell based studies reveal that MEK appears to be activated at higher inhibitor concentrations (Figure 6C), suggesting that high inhibitor concentration may lead to the transactivation of BRAF/CRAF dimers as has been noted elsewhere.[20,21] Given this observation, the further development of these inhibitors could take two paths. In one scenario, these inhibitors could be further optimizated toward increased $BRAF^{V600E}$ potency and specificity to develop an alternative $BRAF^{V600E}$ inhibitor that might have more favorable properties than other $BRAF^{V600E}$ selective inhibitors. Greater $BRAF^{V600E}$ potency and specificity could be achieved by further filling the BRAF/$BRAF^{V600E}$ specificity pocket (Figure 7). Alternatively, these inhibitors could be optimized to also inhibit CRAF, as our kinase profiling studies do show some inhibition of **40** against CRAF. Such compounds might be particularly effective against the reactivation of MAPK pathway activity through the transactivation of BRAF/CRAF dimers. Taken together, this study has resulted in the identification of a new lead series of BRAF inhibitors with the potential for further preclinical development for therapeutic use in melanoma.

EXPERIMENTAL SECTION

Protein Expression and Purification. The human BRAF kinase domain and the V600E containing mutant ($BRAF^{WT}$ and $BRAF^{V600E}$, residues 433−726) with an N-terminal 6X-His tag ($MDRGSH_6GS$) to facilitate protein purification (in the presence of full-length mouse p50cdc37 to faciliate the proper folding of the BRAF kinase) was expressed in Sf9 cells and purified to homogeneity as previously described.[19] The protein was stored at 1.5 mg/mL at 4 °C until use. GST-MEK-His protein was overexpressed at 37 °C in *Escherichia coli* BL21 (Gold) cells as previously described.[19] The protein was stored at 10 mg/mL at −80 °C until use.

In Vitro ELISA-Based Kinase Assay. Recombinantly expressed GST MEK-His, diluted in TTBS buffer [20 mM Tris (pH 7.5), 150 mM NaCl, and 0.05% Tween 20] to 50 μg/mL in a volume of 100 μL, was bound to the wells of a 96-well glutathione-coated plate (Pierce Biotechnology). One microliter of compound (as racemic mixtures) with 2 serial dilutions in a 100% DMSO stock solution was added to a mixture of 50 μL of a buffer containing 50 mMHEPES (pH7.0) with 0.7 pmol of $BRAF^{V600E}$ kinase. This mixture was incubated at room temperature for 1 h before it was added to the GST-MEK-His-bound wells of the 96-well plate. An additional 50 μL of phosphorylation buffer [50 mM HEPES (pH 7.0), 200 mM NaCl, 10 mM $MgCl_2$, and 200 μM ATP] was added to the well mixture to start the kinase reaction at 37 °C for 30 min with intermittent shaking. The kinase reaction was stopped by extensive washing with TTBS buffer, and a 1:5000 dilution of antiphospho-MEK1 (Ser218/222)/MEK2 (Ser222/226) monoclonal antibody (Millipore) in TTBS buffer was subsequently added to the wells and incubated for 1 h with shaking. Goat antirabbit IgG (H+L)-HRP conjugate (Bio-Rad Laboratories) in a 1:5000 dilution was added to the wells for incubation at room temperature with shaking. Finally, the SuperSignal ELISA Pico chemiluminescent substrate (Pierce Biotechnology) was added to the wells. The luminescence signal was recorded with a luminescence filter using a Wallac 1420 luminometer (PerkinElmer).

High throughput inhibitor screening was performed at the Broad Institute of Harvard and MIT Screening Center. Assays were conducted in glutathione coated 384-well plates and followed the procedures essentially as described above but using a 50 μL reaction volume instead of a 100 μL reaction volume to fit the 384-well plate format. Specifically, GST-MEK protein diluted in TTBS to 50 μg/mL was dispensed into the wells of the glutathione coated 384-well plate to a final volume of 50 μL/well using a Matrix Wellmate Dispanser with a microplate stacker (Thermo Scientific). Each plate was agitated using an orbital shaker at 2,500 rpm for 1 min and incubated at room temperature for 1 h. Plates were aspirated and washed once using a wash program with vigorous agitation using an automated microplate washer (Biotek). Then, 3.5 pmol of $BRAF^{V600E}$ kinase domain diluted in 25 μL of 50 mM HEPES at pH 7.5 buffer was added into each well of the plate using the Matrix Wellmate Dispanser, and 25 nL of individual compound (10 mM in 100% DMSO) was transferred into the solution using a Cybi-Well pin-transfer station (Cybio). Plates were agitated using an orbital shaker for 1 min and incubated at room temperature for 1 h. Twenty-five microliters of phosphorylation buffer was then added into the wells to start the kinase reaction (controls were tested to ensure the precise timing for the start of the kinase reaction). Kinase reactions were conducted at room temperature for 30 min and stopped by washing using the microplate washer. A 1:5,000 dilution of Antiphospho-MEK1 (Ser218/222)/MEK2 (Ser222/226) monoclonal antibody (Millipore) in TTBS buffer was subsequently dispensed into the wells to a final volume of 50 μL and incubated for 1 h with shaking. Goat antirabbit IgG (H+L)-HRP conjugate (BioRad Laboratories) in a 1:5,000 dilution was then dispensed into the wells to a final volume of 50 μL to incubate at room temperature with agitation. Finally, 50 μL of the SuperSignal ELISA Pico chemiluminescent substrate (Pierce Biotechnology) was dispensed into the wells to generate the chemiluminescence signal, which was detected using a 700 nm luminescence filter by an Envision chemiluminescence detector (PerkinElmer). A total of 31,976 compounds were screened in duplicate including libraries of a diversity oriented synthesis (DOS), commercially available drug-like compounds, bioactive compounds, natural products, and compounds collected from academic organic synthesis laboratories and a ChemBridge Kinase inhibitor biased library. Compounds were ranked based on a composite Z-score of both duplicates, and the top 100 compounds were cherry-picked from the compound plates at the Broad Institute, and they were reanalyzed by the same assay to confirm their inhibitory activities. According to the results, the top 23 compounds that were deemed to have drug-like properties were confirmed by reordering the compounds from their source vendors and confirming their inhibitor activities.

IC_{50} Value Determination. For IC_{50} calculations of the related quinolol and naphthol inhibitors, the same assay described above was used at different inhibitor concentrations to generate a sigmoidal dose−response curve using $BRAF^{V600E}$ or $BRAF^{WT}$ protein. All dose−response measurements were carried out in duplicate or triplicate, and IC_{50} values were derived from fitting the data to a sigmoidal dose−response curve with a four-parameter logistic model using GraphPad Prism.

Crystallization, Data Collection, and Structure Determination of the Kinase/Inhibitor Complex. Compound **1** dissolved in 100% DMSO was added to 1.5 mg/mL $BRAF^{WT}$ solution in 4-fold molar excess, and this mixture was incubated at room temperature for 1 h before the precipitate was removed by high speed centrifugation. The supernatant was used in the crystallization trials. Crystals were obtained by mixing 1.35 μL of the $BRAF^{WT}$/**1** complex with 1.35 μL of crystallization reservoir solution containing 200 mM magnesium

dx.doi.org/10.1021/jm3004416 | *J. Med. Chem.* 2012, 55, 5220−5230

acetate tetrahydrate, 100 mM sodium cacodylate trihydrate, pH 6.5, and 20% polyethylene glycol (PEG) 8,000) (Hampton Research) supplemented with 0.3 μL of 100 mM nicotinamide adenine dinucleotide (Hampton Research) as an additive by the microbatch method underneath 6 mL of light mineral oil (Sigma) in a 12 × 6 microbatch plate (Hampton Research). Crystals reached a maximum size of 30 μm × 30 μm × 300 μm after about 1 week. Crystals were washed and harvested in cryoprotecting harvest solution containing 200 mM magnesium acetate tetrahydrate, 100 mM sodium cacodylate trihydrate, pH 6.5, 25% PEG 8,000, and 15% glycerol, and flash frozen in liquid propane. Data was collected at beamline GM/CA-CAT 23ID-B at the Advanced Photon Synchrotron Source (Argonne National Laboratory). We discovered that although the crystals showed diffraction to 3.5 Å using a typical X-ray beam (300 μm), they suffered very badly from radiation decay. We were not able to collect more than 5 frames of diffraction data using this size X-ray beam. In contrast, we found that by using an X-ray beam of 10 by 10 μm (minibeam setup at APS beamline 23ID-B), we were able to collect about 20−30 images per crystal position, and both the resolution and mosaicity were significantly improved. Also, importantly, the minibeam setup allowed us to move the beam center to new, unexposed parts of the crystal, allowing us to collect a complete data set from a single crystal. Diffraction data was indexed, integrated, and scaled using the HKL2000 package (HKL Research) and was further processed using the CCP4 program suite.[22]

The structure was determined by molecular replacement using the program Molrep[23] from the CCP4 suite using a previously determined BRAF structure (PDB ID: 1UWH) as a search model. The spacegroup was determined to be $P4_12_12$, and each asymmetric unit contained two molecules. Electron density corresponding to the organic BRAF inhibitor **1** was well resolved in both molecules of the asymmetric unit, and the ligand model was placed into the electron density from the calculated $F_o - F_c$ map and adjusted in Coot.[24] Parameter and topology files for **1** used in the refinements were generated from the HIC-UP XDICT server (http://alpha2.bmc.uu.se/hicup/xdict.html). This was followed by additional refinement using CNS,[25] and the final model was checked for errors using an CNS composite omit map for the protein model and a simulated annealing omit map for inhibitor. The final model was refined with excellent geometry and refinement statistics (Table 1).

Compounds and Chemical Synthesis. *General.* Solvents used for extraction and purification were HPLC grade from Fisher. Unless otherwise indicated, all reactions were run under an inert atmosphere of argon. Anhydrous tetrahydrofuran, ethyl ether, and toluene were obtained via passage through an activated alumina column. Merck precoated silica gel plates (250 mm, 60 F254) were used for analytical TLC. Spots were visualized using 254 nm ultraviolet light, with either anisaldehyde or potassium permanganate stains as visualizing agents. Chromatographic purifications were performed on Sorbent Technologies silica gel (particle size 32−63 μm). ^{1}H and ^{13}C NMR spectra were recorded at 500 and 125 MHz, or 360 and 90 MHz, respectively, in $CDCl_3$, DMSO-d_6, or CD_3OD on a Bruker AM-500, a DRX-500, or a DMX-360 spectrometer. Chemical shifts are reported relative to internal chloroform (d 7.26 for ^{1}H, d 77.0 for ^{13}C), DMSO-d_6 (d 2.50 for ^{1}H, d 39.5 for ^{13}C), or CD_3OD (d 3.31 for ^{1}H, d 49.0 for ^{13}C). Infrared spectra were recorded on a NaCl plate using a Perkin-Elmer 1600 series Fourier transform spectrometer. High resolution mass spectra were obtained by Dr. Rakesh Kohli at the University of Pennsylvania Mass Spectrometry Service Center on an Autospec high resolution double-focusing electrospray ionization/chemical ionization spectrometer with either the DEC 11/73 or OPUS software data system. Melting points were obtained on a Thomas-Hoover capillary melting point apparatus and are uncorrected. On the basis of the analytical methods described above, all compounds were judged to have purities of ≥95%.

General procedure for the synthesis of naphthol derivatives was adapted from WO 2010/005534.[26] Unless otherwise specified, analogues were synthesized using the general procedure.

Compound **2**: Spectroscopic data was identical to that reported previously (WO Patent 2010/005534, January 14, 2010).[26]

Compound **24**: Spectroscopic data was identical to that reported previously (WO Patent 2010/005534, January 14, 2010).[26]

Compound **25**: To a mixture of 4-amino-1-naphthol·HCl (0.196 g, 1.00 mmol), pyridine (0.17 mL, 2.1 mmol), and DMAP (0.005 g, 0.04 mmol) in CH_2Cl_2 was added 2-thiopenesulfonyl chloride (0.194 g, 1.06 mmol). The mixture was heated at reflux for 18 h. The mixture was allowed to cool to 25 °C, and the solvent was removed in vacuo. The resulting residue was diluted with EtOAc (20 mL), and the solution was washed with water (2 × 10 mL), washed with brine, dried over Na_2SO_4, filtered, and concentrated to afford a brown residue. The residue was purified by flash chromatography (5:95 MeOH/CH_2Cl_2) to afford the product as a tan solid (0.240 g, 79%). ^{1}H NMR (500 MHz, DMSO-d_6) δ 10.32 (s, 1H), 9.99 (s, 1H), 8.10−8.08 (m, 1H), 7.84 (dd, J = 5.0, 1.4 Hz, 2H), 7.43−7.37 (m, 2H), 7.35 (dd, J = 3.7, 1.4 Hz, 1H), 7.06 (dd, J = 5.0, 3.7 Hz, 1H), 6.97 (d, J = 8.1 Hz, 1H), 6.76 (d, J = 8.1 Hz, 1H); ^{13}C NMR (125 MHz, DMSO-d_6) δ 153.3, 141.3, 133.5, 132.6, 132.2, 128.1, 126.8, 126.6, 125.5, 125.4, 123.6, 123.4, 122.7, 107.9; IR (thin film) 3268, 3115, 1699, 1584, 1317, 1153, 1016, 774 cm^{-1}; HRMS (ESI) m/z calcd for $C_{14}H_{11}NO_3NaS_2$ $(M + Na)^+$ 328.0078; found, 328.0078.

Compound **26**: To a solution of 2-chloro-1,4-naphthoquinone[27] (0.119 g, 0.50 mmol) and 2-thiophene sulfonamide (0.098 g, 0.60 mmol) cooled to 0 °C in THF (1.8 mL) was added the titanium(IV) chloride tetrahydrofuran complex (0.200 g, 0.60 mmol), followed by the addition of triethylamine (0.18 mL, 1.3 mmol). The mixture was allowed to warm to 25 °C and was heated to 60 °C using a microwave (80 W) for 1 h. The mixture was cooled to 25 °C and added to EtOAc (20 mL). The mixture was filtered though a pad of Celite with EtOAc. The filtrate was concentrated to dryness in vacuo. The resultant residue was suspended in CH_2Cl_2 (10 mL) and filtered though a pad of Celite. The filtrate was concentrated in vacuo to dryness, and the resulting residue was suspended in EtOAc (10 mL). To the suspension was added $Na_2S_2O_4$ (0.436 g, 2.50 mmol) followed by H_2O (5 mL). The mixture was stirred at 25 °C for 1 h. The layers were separated, and an aqueous layer was extracted with EtOAc (3 × 10 mL). The combined organic layers were washed with brine (25 mL), dried over Na_2SO_4, filtered, and concentrated to afford a brown residue. The residue was purified by flash chromatography (40:60 EtOAc/hexanes) to afford the product as a tan solid (0.081 g, 47%). ^{1}H NMR (500 MHz, DMSO-d_6) δ 10.27 (s, 2H), 8.17 (d, J = 8.3 Hz, 1H), 7.87 (d, J = 8.4 Hz, 1H), 7.83 (d, J = 4.4 Hz, 1H), 7.50 (d, J = 7.6 Hz, 1H), 7.46−7.41 (m, 2H), 7.07 (s, 1H), 7.05 (s, 1H);); ^{13}C NMR (125 MHz, DMSO-d_6) δ 148.4, 140.5, 133.9, 133.1, 130.7, 128.3, 127.3, 127.0, 126.54, 126.47, 125.0, 123.8, 122.8, 113.7; IR (thin film) 3276, 1581, 1458, 1401, 1315, 1153, 849, 759 cm^{-1}; HRMS (ESI) m/z calcd for $C_{14}H_9NO_3S_2Cl$ $(M - H)^-$ 337.9712; found, 337.9714.

Compound **27**: To a solution of 2-bromo-1,4-naphthoquinone[28] (0.119 g, 0.50 mmol) and 2-thiophene sulfonamide (0.098 g, 0.60 mmol) cooled to 0 °C in THF (1.8 mL) was added the titanium(IV) chloride tetrahydrofuran complex (0.200 g, 0.60 mmol), followed by the addition of triethylamine (0.18 mL, 1.3 mmol). The mixture was allowed to warm to 25 °C and was heated to 60 °C using a microwave (80 W) for 1 h. The mixture was cooled to 25 °C and added to EtOAc (20 mL). The mixture was filtered though a pad of Celite with EtOAc. The filtrate was concentrated to dryness in vacuo. The resultant residue was suspended in CH_2Cl_2 (10 mL) and filtered though a pad of Celite. The filtrate was concentrated in vacuo to dryness, and the resulting residue was suspended in EtOAc (10 mL). To the suspension was added $Na_2S_2O_4$ (0.436 g, 2.50 mmol) followed by H_2O (5 mL). The mixture was stirred at 25 °C for 1 h. The layers were separated, and the aqueous layer was extracted with EtOAc (3 × 10 mL). The combined organic layers were washed with brine (25 mL), dried over Na_2SO_4, filtered, and concentrated to afford a brown residue. The residue was purified by flash chromatography (40:60 EtOAc/hexanes) to afford the product as a brown solid (0.036 g, 19%). ^{1}H NMR (500 MHz, DMSO-d_6) δ 10.26 (s, 1H), 10.24 (s, 1H), 8.18 (d, J = 8.4 Hz, 1H), 7.88−7.86 (m, 2H), 7.51 (ddd, J = 8.3, 7.0, 1.2 Hz, 1H), 7.45 (ddd, J = 8.4, 6.9, 1.3 Hz, 1H), 7.40 (dd, J = 3.7, 1.3 Hz, 1H), 7.08 (dd, J = 5.0, 3.7 Hz, 1H), 7.06 (s, 1H); ^{13}C NMR (125 MHz, DMSO-d_6) δ 147.8, 140.1, 133.4, 132.5, 130.1, 127.7, 126.6, 126.3, 126.0, 125.9,

dx.doi.org/10.1021/jm3004416 | J. Med. Chem. 2012, 55, 5220−5230

124.5, 123.3, 122.2, 113.2; IR (thin film) 3479, 3098, 1582, 1459, 1415, 1315, 1154, 759 cm^{-1}; HRMS (ESI) m/z calcd for $C_{14}H_9NO_3S_2Cl$ $(M - HBr + Cl)^-$ 337.9712; found, 337.9707.

28: ^1H NMR (500 MHz, DMSO-d_6) δ 10.09 (s, 1H), 8.20 (d, J = 8.0 Hz, 1H), 7.88−7.82 (m, 2H), 7.53−7.47 (m, 1H), 7.47−7.41 (m, 1H), 7.31 (dd, J = 1.5, 3.5 Hz, 1H), 7.21 (s, 2H), 7.05 (dd, J = 3.5, 5.0 Hz, 1H), 6.83 (s, 1H); ^{13}C NMR (125 MHz, DMSO-d_6) δ 152.2, 145.1, 137.4, 131.4, 131.0, 129.8, 129.2, 127.2, 126.1, 125.7, 123.9, 123.4, 123.1, 122.6; IR (KBr disk) 3262, 3105, 1709, 1567, 1506, 1451, 1403, 1377, 1325, 1157, 1016, 911, 854, 766, 723, 669 cm^{-1}; HRMS (ESI) m/z calcd for $C_{17}H_{14}N_3O_3S_3$ $(M + H)^+$ 404.0197; found, 404.0204.

Compound **29**: ^1H NMR (500 MHz, $CDCl_3$) δ 10.85 (s, 1H), 8.44 (d, J = 5.0 Hz, 1H), 8.39 (d, J = 7.5 Hz, 1H), 7.76 (d, J = 7.5 Hz, 1H), 7.61 (t, J = 7.5 Hz, 1H), 7.53−7.43 (m, 3H), 7.41 (s, 1H), 7.36 (d, J = 4.0 Hz, 1H), 7.24 (s, 1H), 7.16 (dd, J = 4.0, 7.5 Hz, 1H), 6.89 (dd, J = 3.5, 5.0 Hz, 1H), 6.61 (br s, 1H); ^{13}C NMR (125 MHz, $CDCl_3$) δ 159.8, 156.4, 149.1, 139.8, 138.1, 133.2, 132.6, 131.1, 128.5, 127.5, 126.4, 126.3, 124.0, 123.5, 123.1, 121.9, 121.6, 110.1; IR (KBr disk) 3235, 3062, 2920, 2848, 1564, 1451, 1414, 1374, 1322, 1153, 1070, 1015, 762, 719 cm^{-1}; HRMS (ESI) m/z calcd for $C_{19}H_{14}N_2O_3S_3$ $(M + H)^+$ 415.0245; found, 415.0257.

Compound **30**: Spectroscopic data was identical to that reported previously (WO Patent 2010/005534, January 14, 2010).[26]

Compound **31**: ^1H NMR (500 MHz, $CDCl_3$) δ 8.31 (d, J = 8.0 Hz, 1H), 7.98 (d, J = 8.0 Hz, 1H), 7.62−7.53 (m, 2H), 7.42 (dd, J = 1.0, 5.0 Hz, 1H), 7.35 (dd, J = 1.0, 3.5 Hz, 1H), 7.30−7.16 (m, 5H), 7.10−7.06 (m, 2H), 6.83 (dd, J = 4.0, 5.0 Hz, 1H), 6.62 (br s, 1H); ^{13}C NMR (125 MHz, DMSO-d_6) δ 154.9, 139.4, 135.5, 133.3, 133.0, 132.6, 131.5, 129.4, 128.8, 127.6, 127.4, 126.7, 124.3, 124.0, 123.8, 122.6, 108.9; IR (KBr disk) 3391, 3272, 2920, 2851, 1568, 1435, 1373, 1346, 1311, 1266, 1220, 1156, 1070, 907, 720 cm^{-1}; HRMS (ESI) m/z calcd for $C_{20}H_{15}NNaO_3S_3$ $(M + H)^+$ 436.0112; found, 436.0120.

Compound **32**: ^1H NMR (500 MHz, DMSO-d_6) δ 10.50−9.50 (br, 2H, contains two s), 8.16 (d, J = 8.5 Hz, 1H), 8.15−7.75 (m, 3H, contains one br s; one d, J = 8.5 Hz; one dd, J = 1.5, 5.0 Hz), 7.54−7.47 (m, 1H), 7.47−7.40 (m, 1H), 7.26 (dd, J = 1.5, 3.5 Hz, 1H), 7.02 (dd, J = 3.5, 5.0 Hz, 1H), 6.68 (s, 1H); ^{13}C NMR (125 MHz, DMSO-d_6) δ 140.1, 133.0, 132.1, 130.7, 127.5, 126.4, 126.0, 125.5, 124.6, 123.5, 122.1; IR (KBr disk) 3101, 2991, 2917, 1568, 1506, 1452, 1402, 1376, 1323, 1263, 1156, 1072, 1020, 912, 854, 764, 723, 670 cm^{-1}; HRMS (ESI) m/z calcd for $C_{16}H_{13}N_4O_3S_3$ $(M + H)^+$ 405.0150; found, 405.0166.

Compound **33**: ^1H NMR (500 MHz, DMSO-d_6) δ 10.13 (s, 1H), 9.73 (s, 1H), 8.54 (s, 1H), 8.19−8.17 (m, 1H), 8.02−7.99 (m, 2H), 7.52−7.47 (m, 2H), 7.44−7.42 (m, 1H), 7.40 (d, J = 0.3 Hz, 1H), 6.89 (s, 1H), 4.11 (t, J = 8.5 Hz, 2H), 3.06 (t, J = 8.4 Hz, 2H), 2.18 (s, 3H); ^{13}C NMR (125 MHz, DMSO-d_6) δ 169.9, 135.1, 134.7, 134.1, 133.1, 127.3, 127.2, 126.5, 126.3, 126.2, 126.0, 124.1, 123.9, 123.8, 122.8, 115.4, 113.6, 111.3, 49.0, 27.2, 24.5; IR (thin film) 3121, 2924, 1708, 1660, 1481, 1397, 1149, 1072 cm^{-1}; HRMS (ESI) m/z calcd for $C_{22}H_{19}N_5O_4NaS_2$ $(M + Na)^+$ 504.0776; found, 504.0788.

Compound **34**: ^1H NMR (500 MHz, DMSO-d_6) δ 14.00 (br s, 1H), 10.80−9.60 (br s, 2H), 8.46 (br s, 1H), 8.18 (d, J = 8.0 Hz, 1H), 7.93−7.73 (m, 5H), 7.55−7.37 (m, 2H), 6.88 (br s, 1H); ^{13}C NMR (125 MHz, DMSO-d_6) δ 152.2, 145.1, 143.5, 132.7, 132.4, 132.2, 131.3, 129.1, 127.7, 126.9, 126.2, 126.1, 125.9, 125.6, 124.5, 123.8, 123.2, 122.6, 122.3; ^{19}F NMR (470 MHz, DMSO-d_6) δ −61.6; IR (KBr disk) 3102, 2989, 2928, 1730, 1568, 1504, 1453, 1403, 1376, 1322, 1267, 1168, 1062, 762, 711 cm^{-1}; HRMS (ESI) m/z calcd for $C_{19}H_{14}F_3N_4O_3S_2$ $(M + H)^+$ 467.0459, found: 467.0471.

Compound **35**: ^1H NMR (500 MHz, DMSO-d_6) δ 9.42 (s, 1H), 8.49 (s, 1H), 8.23 (d, J = 8.1 Hz, 1H), 8.17 (d, J = 8.5 Hz, 1H), 7.62−7.55 (m, 2H), 7.29 (s, 1H), 3.00 (dd, J = 7.9, 7.7 Hz, 2H), 1.70−1.64 (m, 2H), 1.30−1.17 (m, 14H), 0.85 (t, J = 6.9 Hz, 3H); ^{13}C NMR (125 MHz, DMSO-d_6) δ 151.9, 133.1, 132.1, 131.6, 130.2, 128.7 127.1, 126.0, 125.0, 124.5, 123.8, 122.6, 50.7, 31.3, 28.87, 28.68, 28.48, 27.5, 23.1, 22.1, 14.0; IR (thin film) 2923, 2853, 1567, 1454, 1279, 1141, 1076, 767 cm^{-1}; HRMS (ESI) m/z calcd for $C_{22}H_{30}N_4O_3NaS_2$ $(M + Na)^+$ 485.1657; found, 485.1656.

Compound **36**: ^1H NMR (500 MHz, DMSO-d_6) δ 10.23 (s, 1H), 9.44 (s, 1H), 8.62 (s, 1H), 8.24 (d, J = 8.3 Hz, 1H), 8.18 (d, J = 8.1 Hz, 1H), 7.62−7.55 (m, 2H), 7.31 (s, 1H), 3.01 (t, J = 7.8 Hz, 2H), 1.71−1.65 (m, 2H), 1.30−1.19 (m, 10H), 0.84 (t, J = 7.0 Hz, 3H); ^{13}C NMR (125 MHz, DMSO-d_6) δ 145.1, 140.5, 134.4, 131.6, 127.2, 127.1, 126.1, 125.8, 123.9, 122.6, 50.7, 31.2, 28.5, 28.4, 27.5, 23.2, 22.1, 14.0; IR (thin film) 3253, 2925, 2855, 1568, 1454, 1279, 1141, 766 cm^{-1}; HRMS (ESI) m/z calcd for $C_{20}H_{26}N_4O_3NaS_2$ $(M + Na)^+$ 457.1344; found, 457.1325.

Compound **37**:^1H NMR (500 MHz, CD_3OD) δ 8.25 (dt, J = 4.4, 2.4 Hz, 1H), 8.19 (s, 1H), 8.06 (dt, J = 4.3, 2.4 Hz, 1H), 7.42−7.41 (m, 2H), 7.38 (s, 1H), 7.18−7.08 (m, 10H), 6.90 (dt, J = 8.8, 4.4 Hz, 1H), 6.63 (t, J = 9.4 Hz, 1H), 4.02 (s, 4H); ^{13}C NMR (125 MHz, CD_3OD) δ 156.2, 155.7, 155.3, 154.2, 153.3, 138.6, 137.1, 133.5, 130.8, 129.3, 128.9, 128.6, 128.5, 128.2, 127.2, 127.1, 125.2, 124.3, 123.8, 119.1, 112.8, 112.6, 68.8, 57.0, 26.4; IR (thin film) 3087, 2924, 1705, 1570, 1485, 1364, 1171, 745 cm^{-1}; HRMS (ESI) m/z calcd for $C_{32}H_{25}N_5O_3F_2NaS_2$ $(M + Na)^+$ 652.1265; found, 652.1271.

Compound **38**: ^1H NMR (500 MHz, DMSO-d_6) δ 10.98 (s, 1H), 10.38 (s, 1H), 8.59 (s, 1H), 8.24−8.22 (m, 1H), 7.99 (s, 1H), 7.58 (s, 2H), 6.97 (s, 1H); ^{13}C NMR (125 MHz, DMSO-d_6) δ 157.1, 152.4, 145.5, 143.2, 138.8, 136.8, 131.8, 128.8, 127.7, 126.7, 126.1, 123.5, 123.0, 115.6, 112.1; IR (thin film) 3129, 2928, 1704, 1520, 1502, 1176, 1101, 992 cm^{-1}; HRMS (ESI) m/z calcd for $C_{18}H_{10}N_4O_3F_5S_2$ $(M + H)^+$ 489.0115; found, 489.0110.

Compound **39**: ^1H NMR (500 MHz, DMSO-d_6) δ 10.76 (s, 1H), 10.31 (s, 1H), 8.57 (s, 1H), 8.23−8.21 (m, 1H), 7.93 (dd, J = 6.6, 2.9 Hz, 1H), 7.69−7.65 (m, 1H), 7.53 (dd, J = 6.4, 3.2 Hz, 2H), 7.32 (t, J = 9.0 Hz, 1H), 7.16 (s, 1H), 2.90−2.82 (m, 4H); ^{13}C NMR (125 MHz, DMSO-d_6) δ 176.2, 159.6, 157.5, 155.4, 153.3, 145.5, 135.6, 131.8, 129.8, 127.7, 126.4, 126.0, 123.4, 123.0, 119.0, 118.4, 114.0, 113.7, 29.1; IR (thin film) 2920, 2848, 1719, 1592, 1562, 1492, 1298, 1172 cm^{-1}; HRMS (ESI) m/z calcd for $C_{22}H_{15}N_5O_5NaS_2F_2$ $(M + Na)^+$ 554.0380; found, 554.0386.

Compound **40**: To a solution of 2-chloro-1,4-naphthoquinone[27] (0.096 g, 0.50 mmol) and biphenyl-4-sulfonamide (0.140 g, 0.60 mmol) cooled to 0 °C in THF (1.8 mL) was added the titanium(IV) chloride tetrahydrofuran complex (0.200 g, 0.60 mmol), followed by the addition of triethylamine (0.18 mL, 1.3 mmol). The mixture was allowed to warm to 25 °C and was heated to 60 °C using a microwave (80 W) for 1 h. The mixture was cooled to 25 °C and added to EtOAc (20 mL). The mixture was filtered though a pad of Celite with EtOAc. The filtrate was concentrated to dryness in vacuo. The resultant residue was suspended in CH_2Cl_2 (10 mL) and filtered though a pad of Celite. The filtrate was concentrated to dryness and then dissolved in THF (10 mL). To the solution was added 1*H*-1,2,4-triazole-3-thiol (0.051 g, 0.50 mmol), and the mixture was stirred at 25 °C for 4 h. The mixture was concentrated in vacuo to dryness, and the resultant residue was suspended in EtOAc (10 mL). To the suspension was added $Na_2S_2O_4$ (0.436 g, 2.50 mmol) followed by H_2O (5 mL). The mixture was stirred at 25 °C for 1 h. The layers were separated, and the aqueous layer was extracted with EtOAc (3 × 10 mL). The combined organic layers were washed with brine (25 mL), dried over Na_2SO_4, filtered, and concentrated to afford a brown residue. The residue was purified by flash chromatography (3:97 MeOH/CH_2Cl_2) to afford the product as a colorless solid (0.111 g, 47%): ^1H NMR (500 MHz, DMSO-d_6) δ 10.22 (s, 0.5H), 9.98 (s, 1H), 8.54 (s, 0.5H), 8.19 (d, J = 7.9 Hz, 1H), 7.97 (d, J = 8.0 Hz, 1H), 7.74 (d, J = 8.5 Hz, 2H), 7.68 − 7.66 (m, 5H), 7.51−7.41 (m, 6H), 6.96 (s, 1H); ^{13}C NMR (125 MHz, DMSO-d_6) δ 144.1, 138.6, 138.4, 129.2, 128.5, 127.5, 127.2, 127.1, 127.0, 126.0, 125.7, 123.5, 122.6; IR (thin film) 3249, 2923, 1704, 1593, 1452, 1320, 1160, 763 cm^{-1}; HRMS (ESI) m/z calcd for $C_{24}H_{18}N_4O_3NaS_2$ $(M + Na)^+$ 497.0718; found, 497.0711.

Compound **41**: ^1H NMR (360 MHz, DMSO-d_6) δ 14.11 (br s, 1H), 10.60−9.70 (br s, 2H), 8.32 (br s, 1H), 8.21 (s, 1H), 8.15 (d, J = 8.0 Hz, 1H), 8.15−7.75 (m, 4H), 7.80−7.55 (m, 3H), 7.55−7.30 (m, 2H), 6.92 (br s, 1H); ^{13}C NMR (125 MHz, DMSO-d_6) δ 151.8, 145.0, 136.9, 134.1, 131.5, 131.4, 129.2, 129.1, 128.7, 128.6, 127.8, 127.7, 127.5, 126.8, 125.9, 125.6, 124.4, 123.5, 122.4, 122.3; IR (KBr disk) 3259, 3053, 2851, 1564, 1508, 1468, 1450, 1347, 1318, 1285, 1156,

1026, 945, 766, 666 cm^{-1}; HRMS (ESI) m/z calcd for $C_{22}H_{17}N_4O_3S_2$ $(M + H)^+$ 449.0742; found, 449.0753.

Kinase Specificity Profile. The kinase assays for PAK1, PIM1, GS3Kα, PI3Kα, and PI3Kγ were carried out as described previously,[29] and CRAF was assayed as described above for BRAF using between 20 and 30 nM enzyme and 100 μM ATP .

The p70S6K kinase assay was performed using labeled γ-P^{32} ATP, and the incorporation of labeled phosphate onto substrate (S6 kinase/Rsk2 peptide) was monitored. Various concentrations of inhibitor were incubated at room temperature in 20 mM MOPS, 30 mM $MgCl_2$, 0.8 μg/μL BSA, and 5% DMSO (resulting from the inhibitor stock solution), pH 7.0, in the presence of substrate (S6 kinase/Rsk2 substrate peptide 2: 3.6 μM) and p70S6K kinase (20nM). After 15 min, the reaction was initiated by adding ATP to a final concentration of 100 μM, including approximately 0.4 μCi/μL γ-P^{32} ATP. Reactions were performed in a total volume of 25 μL. After 30 min, the reaction was terminated by spotting 17.5 μL on a circular P81 phosphocellulose paper (diameter 2.1 cm, Whatman) followed by washing four times (five minutes each wash) with 0.75% phosphoric acid and once with acetone. The dried P81 papers were transferred to a scintillation vial with 5 mL of scintillation cocktail and the counts per minute (CPM) determined with a Beckmann 6000 scintillation counter. IC_{50} values were defined to be the concentration of inhibitor at which the CPM was 50% of the control sample, corrected by the background.

Melanoma Proliferation Assay. The human melanoma cell line (451Lu) was isolated as previously described[30] and cultured in Dulbecco's modified Eagle's medium supplemented with 5% fetal bovine serum. Normal human primary melanocytes (FOM) and fibroblasts (FF) were isolated from the human epidermis of neonatal foreskins and cultured as described.[31] Cells (5000/well) were seeded in 96-well plates and allowed to adhere overnight before treatment with **40** or the DMSO vehicle control for 72 h. Cells were then directly incubated with MTS substrate (CellTiter-96 Aqueous One Solution Cell Proliferation Assay, Promega). Absorbance was measured at 490 nm as per the supplier's instructions, and percent proliferation was normalized to the absorbance of DMSO-treated cells. For each experiment, cell line, and treatment, the absorbance values of at least 4 wells were used for data analysis, and the experiment was conducted in triplicate.

Western Blot Analyses. Proteins were extracted and immunoblotted as previously described.[32] Antibodies to phospho-MEK, total-MEK, phospho-ERK, total-ERK, and HSP90 were from Cell Signaling Technology (Beverly, MA).

■ ASSOCIATED CONTENT

Supporting Information

Supplemental methods, references, confirmation of the top 30 compounds as hits from the HTS experiments; twenty-three compounds showing drug-like structures identified from the HTS against $BRAF^{V600E}$; and structures and IC_{50} values of additional naphthol inhibitor analogues against $BRAF^{WT}$ and $BRAF^{V600E}$. This material is available free of charge via the Internet at http://pubs.acs.org.

Accession Codes

PDB ID code: $BRAF^{V600E}$/inhibitor **1** complex (pdb ID: 4E26) is available at the Protein Data Bank.

■ AUTHOR INFORMATION

Corresponding Author

*(J.W.) Department of Chemistry, University of Pennsylvania, Philadelphia, PA 19104. Phone: 215-898-0052. Fax: 215-573-2112. E-mail: winkler@sas.upenn.edu. (R.M.) The Wistar Institute, 3601 Spruce Street, Philadelphia, PA 19104. Phone: 215-898-5006. Fax: 215-898-0381. E-mail: marmor@wistar.org

Notes

The authors declare no competing financial interest.

■ ACKNOWLEDGMENTS

We thank Jessie Villanueva for useful discussions. This work was supported by NIH grant CA114046 awarded to M.H., R.M. and J.W. This project was also funded in part with Federal funds from the National Cancer Institute's Initiative for Chemical Genetics, National Institutes of Health, under Contract No. N01-CO-12400 with some experiments performed with the assistance of the Chemical Biology Platform of the Broad Institute of Harvard and MIT. We acknowledge support of the Protein Expression and Libraries Core Facility at the Wistar Institute, which is supported by NIH grant CA010815.

■ REFERENCES

(1) Wellbrock, C.; Karasarides, M.; Marais, R. The RAF proteins take centre stage. *Nat. Rev. Mol. Cell. Biol.* **2004**, *5*, 875−885.

(2) Wojnowski, L.; Stancato, L. F.; Larner, A. C.; Rapp, U. R.; Zimmer, A. Overlapping and specific functions of Braf and Craf-1 proto-oncogenes during mouse embryogenesis. *Mech. Dev.* **2000**, *91*, 97−104.

(3) Jaiswal, R. K.; Moodie, S. A.; Wolfman, A.; Landreth, G. E. The mitogen-activated protein kinase cascade is activated by B-Raf in response to nerve growth factor through interaction with p21ras. *Mol. Cell. Biol.* **1994**, *14*, 6944−6953.

(4) Davies, H.; Bignell, G. R.; Cox, C.; Stephens, P.; Edkins, S.; Clegg, S.; Teague, J.; Woffendin, H.; Garnett, M. J.; Bottomley, W.; Davis, N.; Dicks, E.; Ewing, R.; Floyd, Y.; Gray, K.; Hall, S.; Hawes, R.; Hughes, J.; Kosmidou, V.; Menzies, A.; Mould, C.; Parker, A.; Stevens, C.; Watt, S.; Hooper, S.; Wilson, R.; Jayatilake, H.; Gusterson, B. A.; Cooper, C.; Shipley, J.; Hargrave, D.; Pritchard-Jones, K.; Maitland, N.; Chenevix-Trench, G.; Riggins, G. J.; Bigner, D. D.; Palmieri, G.; Cossu, A.; Flanagan, A.; Nicholson, A.; Ho, J. W.; Leung, S. Y.; Yuen, S. T.; Weber, B. L.; Seigler, H. F.; Darrow, T. L.; Paterson, H.; Marais, R.; Marshall, C. J.; Wooster, R.; Stratton, M. R.; Futreal, P. A. Mutations of the BRAF gene in human cancer. *Nature* **2002**, *417*, 949−954.

(5) Greenman, C.; Stephens, P.; Smith, R.; Dalgliesh, G. L.; Hunter, C.; Bignell, G.; Davies, H.; Teague, J.; Butler, A.; Stevens, C.; Edkins, S.; O'Meara, S.; Vastrik, I.; Schmidt, E. E.; Avis, T.; Barthorpe, S.; Bhamra, G.; Buck, G.; Choudhury, B.; Clements, J.; Cole, J.; Dicks, E.; Forbes, S.; Gray, K.; Halliday, K.; Harrison, R.; Hills, K.; Hinton, J.; Jenkinson, A.; Jones, D.; Menzies, A.; Mironenko, T.; Perry, J.; Raine, K.; Richardson, D.; Shepherd, R.; Small, A.; Tofts, C.; Varian, J.; Webb, T.; West, S.; Widaa, S.; Yates, A.; Cahill, D. P.; Louis, D. N.; Goldstraw, P.; Nicholson, A. G.; Brasseur, F.; Looijenga, L.; Weber, B. L.; Chiew, Y. E.; DeFazio, A.; Greaves, M. F.; Green, A. R.; Campbell, P.; Birney, E.; Easton, D. F.; Chenevix-Trench, G.; Tan, M. H.; Khoo, S. K.; Teh, B. T.; Yuen, S. T.; Leung, S. Y.; Wooster, R.; Futreal, P. A.; Stratton, M. R. Patterns of somatic mutation in human cancer genomes. *Nature* **2007**, *446*, 153−158.

(6) Ikenoue, T.; Hikiba, Y.; Kanai, F.; Tanaka, Y.; Imamura, J.; Imamura, T.; Ohta, M.; Ijichi, H.; Tateishi, K.; Kawakami, T.; Aragaki, J.; Matsumura, M.; Kawabe, T.; Omata, M. Functional analysis of mutations within the kinase activation segment of B-Raf in human colorectal tumors. *Cancer Res.* **2003**, *63*, 8132−8137.

(7) Satyamoorthy, K.; Li, G.; Gerrero, M. R.; Brose, M. S.; Volpe, P.; Weber, B. L.; Van Belle, P.; Elder, D. E.; Herlyn, M. Constitutive mitogen-activated protein kinase activation in melanoma is mediated by both BRAF mutations and autocrine growth factor stimulation. *Cancer Res.* **2003**, *63*, 756−759.

(8) Dienstmann, R.; Tabernero, J. BRAF as a target for cancer therapy. *Anticancer Agents Med. Chem.* **2011**, *11*, 285−295.

(9) Finn, L.; Markovic, S. N.; Joseph, R. W. Therapy for metastatic melanoma: the past, present, and future. *BMC Med.* **2012**, *10*, 23.

(10) Zambon, A.; Niculescu-Duvaz, I.; Niculescu-Duvaz, D.; Marais, R.; Springer, C. J. Small molecule inhibitors of BRAF in clinical trials. *Bioorg. Med. Chem. Lett.* **2012**, *22*, 789−792.

(11) Wan, P. T. C.; Garnett, M. J.; Roe, S. M.; Lee, S.; Niculescu-Duvaz, D.; Good, V. M.; Project, C. G.; Jones, C. M.; Marshall, C. J.; Springer, C. J.; Barford, D.; Marais, R. Mechanism of activation of the RAF-ERK signaling pathway by oncogenic mutations of B-Raf. *Cell* **2004**, *116*, 855−867.
(12) Chapman, P. B.; Hauschild, A.; Robert, C.; Haanen, J. B.; Ascierto, P.; Larkin, J.; Dummer, R.; Garbe, C.; Testori, A.; Maio, M.; Hogg, D.; Lorigan, P.; Lebbe, C.; Jouary, T.; Schadendorf, D.; Ribas, A.; O'Day, S. J.; Sosman, J. A.; Kirkwood, J. M.; Eggermont, A. M.; Dreno, B.; Nolop, K.; Li, J.; Nelson, B.; Hou, J.; Lee, R. J.; Flaherty, K. T.; McArthur, G. A. Improved survival with vemurafenib in melanoma with BRAF V600E mutation. *N. Engl. J. Med.* **2011**, *364*, 2507−2516.
(13) Poulikakos, P. I.; Persaud, Y.; Janakiraman, M.; Kong, X.; Ng, C.; Moriceau, G.; Shi, H.; Atefi, M.; Titz, B.; Gabay, M. T.; Salton, M.; Dahlman, K. B.; Tadi, M.; Wargo, J. A.; Flaherty, K. T.; Kelley, M. C.; Misteli, T.; Chapman, P. B.; Sosman, J. A.; Graeber, T. G.; Ribas, A.; Lo, R. S.; Rosen, N.; Solit, D. B. RAF inhibitor resistance is mediated by dimerization of aberrantly spliced BRAF(V600E). *Nature* **2011**, *480*, 387−390.
(14) Villanueva, J.; Vultur, A.; Herlyn, M. Resistance to BRAF inhibitors: unraveling mechanisms and future treatment options. *Cancer Res.* **2011**, *71*, 7137−7140.
(15) Niculescu-Duvaz, I.; Roman, E.; Whittaker, S. R.; Friedlos, F.; Kirk, R.; Scanlon, I. J.; Davies, L. C.; Niculescu-Duvaz, D.; Marais, R.; Springer, C. J. Novel inhibitors of B-RAF based on a disubstituted pyrazine scaffold. Generation of a nanomolar lead. *J. Med. Chem.* **2006**, *49*, 407−416.
(16) Luo, C.; Xie, P.; Marmorstein, R. Identification of BRAF inhibitors through in silico screening. *J. Med. Chem.* **2008**, *51*, 6121−6127.
(17) Lipinski, C. A.; Lombardo, F.; Dominy, B. W.; Feeney, P. J. Experimental and computational approaches to estimate solubility and permeability in drug discovery and development settings. *Adv. Drug Delivery Rev.* **2001**, *46*, 3−26.
(18) Tsai, J.; Lee, J. T.; Wang, W.; Zhang, J.; Cho, H.; Mamo, S.; Bremer, R.; Gillette, S.; Kong, J.; Haass, N. K.; Sproesser, K.; Li, L.; Smalley, K. S.; Fong, D.; Zhu, Y. L.; Marimuthu, A.; Nguyen, H.; Lam, B.; Liu, J.; Cheung, I.; Rice, J.; Suzuki, Y.; Luu, C.; Settachatgul, C.; Shellooe, R.; Cantwell, J.; Kim, S. H.; Schlessinger, J.; Zhang, K. Y.; West, B. L.; Powell, B.; Habets, G.; Zhang, C.; Ibrahim, P. N.; Hirth, P.; Artis, D. R.; Herlyn, M.; Bollag, G. Discovery of a selective inhibitor of oncogenic B-Raf kinase with potent antimelanoma activity. *Proc. Natl. Acad. Sci. U.S.A.* **2008**, *105*, 3041−3046.
(19) Xie, P.; Streu, C.; Qin, J.; Bregman, H.; Pagano, N.; Meggers, E.; Marmorstein, R. The crystal structure of BRAF in complex with an organoruthenium inhibitor reveals a mechanism for inhibition of an active form of BRAF kinase. *Biochemistry* **2009**, *48*, 5187−5198.
(20) Heidorn, S. J.; Milagre, C.; Whittaker, S.; Nourry, A.; Niculescu-Duvas, I.; Dhomen, N.; Hussain, J.; Reis-Filho, J. S.; Springer, C. J.; Pritchard, C.; Marais, R. Kinase-dead BRAF and oncogenic RAS cooperate to drive tumor progression through CRAF. *Cell* **2010**, *140*, 209−221.
(21) Poulikakos, P. I.; Zhang, C.; Bollag, G.; Shokat, K. M.; Rosen, N. RAF inhibitors transactivate RAF dimers and ERK signalling in cells with wild-type BRAF. *Nature* **2010**, *464*, 427−430.
(22) project, C. c.; , n. The CCP4 suite: programs for protein crystallography. *Acta Crystallogr., Sect. D* **1994**, *50*, 760−763.
(23) Vagin, A.; Teplyakov, A. MOLREP: an automated program for molecular replacement. *J. Appl. Crystallogr.* **1997**, *30*, 1022−1025.
(24) Emsley, P.; Cowtan, K. Coot: model-building tools for molecular graphics. *Acta Crystallogr.* **2004**, *60*, 2126−2132.
(25) Brunger, A. T.; Adams, P. D.; Clore, G. M.; DeLano, W. L.; Gros, P.; Grosse-Kunstleve, R. W.; Jiang, J. S.; Kuszewski, J.; Nilges, M.; Pannu, N. S.; Read, R. J.; Rice, L. M.; Simonson, T.; Warren, G. L. Crystallography & NMR system: A new software suite for macromolecular structure determination. *Acta Crystallogr., Sect. D* **1998**, *54*, 905−921.
(26) Lawrence, H.; Ge, Y.; Sebti, S. M.; Guida, W.Proteasome Inhibitors for Selectively Inducing Apoptosis in Cancer Cells. US Patent 20110201609, 2010.
(27) Sucunza, D.; Dembkowski, D.; Neufeind, S.; Velder, J.; Lex, J.; Schmalz, H. G. Synthesis of a mumbaistatin analogue through cross-coupling. *Synlett* **2007**, *16*, 2569−2573.
(28) Brimble, M. A.; Bachu, P.; Spery, J. Enantioselective synthesis of an analogue of nanaomycin A. *Synthesis* **2007**, *18*, 2887−2893.
(29) Xie, P.; Williams, D. S.; Atilla-Gokcumen, G. E.; Milk, L.; Xiao, M.; Smalley, K. S.; Herlyn, M.; Meggers, E.; Marmorstein, R. Structure-based design of an organoruthenium phosphatidyl-inositol-3-kinase inhibitor reveals a switch governing lipid kinase potency and selectivity. *ACS Chem. Biol.* **2008**, *3*, 305−316.
(30) Fang, D.; Nguyen, T. K.; Leishear, K.; Finko, R.; Kulp, A. N.; Hotz, S.; Van Belle, P. A.; Xu, X.; Elder, D. E.; Herlyn, M. A tumorigenic subpopulation with stem cell properties in melanomas. *Cancer Res.* **2005**, *65*, 9328−37.
(31) Hsu, M. Y.; Shih, D. T.; Meier, F. E.; Van Belle, P.; Hsu, J. Y.; Elder, D. E.; Buck, C. A.; Herlyn, M. Adenoviral gene transfer of beta3 integrin subunit induces conversion from radial to vertical growth phase in primary human melanoma. *Am. J. Pathol.* **1998**, *153*, 1435−1442.
(32) Vultur, A.; Buettner, R.; Kowolik, C.; Liang, W.; Smith, D.; Boschelli, F.; Jove, R. SKI-606 (bosutinib), a novel Src kinase inhibitor, suppresses migration and invasion of human breast cancer cells. *Mol. Cancer Ther.* **2008**, *7*, 1185−1194.
(33) Krissinel, E.; Henrick, K. Secondary-structure matching (SSM), a new tool for fast protein structure alignment in three dimensions. *Acta Crystallogr.* **2004**, *60*, 2256−2268.